Proceedings of the
International Conference on Mechanical Engineering 2011
(ICME2011) 18-20 December 2011, Dhaka, Bangladesh

ICME11-FL-019

A COMPUTATIONAL STUDY OF BLOCKAGE EFFECTS ON VEHICLE AERODYNAMIC DRAG IN CLOSED-WALL WIND TUNNEL

Prasanjit Das[1], **Makoto Tsubokura**[2], **Tomofuyu Matsuuki**[3], **Nobuyuki Oshima**[4] **and Kozo Kitoh**[5]

[1,2,4]Hokkaido University, Sapporo, Hokkaido, Japan
[3]Isuzu Advanced Engineering center Ltd., Fujisawa, Kanagawa, Japan
[5]Kozo Kitoh Technology, Inc., Japan

ABSTRACT

The combined effects of the various types of blockage on aerodynamic drag in a closed-wall wind tunnel were investigated using computational fluid dynamics (CFD). The large-eddy simulation (LES) method adopted was first validated on a static condition measured at the DNW-German Dutch wind tunnel and satisfactory agreement is attained. The simulation of flow past two different realistic, full-scale, heavy-duty truck models was conducted. The models were placed at different yawing angles in the virtual wind tunnels with blockage ratio of about 10%; which is exactly the same as the experimental wind tunnel geometry. To compare the results with ideal (blockage free condition) case, other simulations with larger cross section at the blockage ratio of 1.1% were also conducted. The empty tunnel simulation was conducted in order to discern the effects of tunnel pressure gradients. Comparisons of the ideal CFD results to the corrected C_d values obtained by some existing blockage correction methods for closed-wall wind tunnel are also examined.

Keywords: Wind Tunnel Blockage, Aerodynamic Drag, Closed-Wall Wind Tunnel, CFD.

1. INTRODUCTION

At the development stage, it is important to assess the drag performance of vehicle, because it is accounted for about 75-80% of total resistance to be overcome by the vehicle's engine power [1]. In a typical class of heavy-duty truck, power required to overcome rolling resistance and accessories increases linearly with vehicle speed, while energy losses due to aerodynamic drag increase with the cube of the speed. At a typical highway speed of 70 mph, aerodynamic drag accounts for approximately 65% of the energy output of the engine. Even modest reductions in aerodynamic drag can significantly reduce fuel consumption. Lower fuel consumption will result in a reduction in pollution emission.

In automotive industry, to assess the performance of road vehicle, aerodynamic testing is normally conducted in wind tunnel. The constraint effects imposed by the walls of a wind tunnel distort the flow field round a model so that the test result does not give an actual representation of conditions in an unconfined flow. Therefore, correction is needed before the measured result can represent the vehicle's performance under actual road condition, which is free from the wall constraint effects.

To date, most of the blockage correction equations of closed-wall wind tunnel were based on simplified bluff body geometry. Cooper et al. [2] compared a number of correction methods and recommended not to use the classical formulae for vehicle aerodynamics. Wind tunnel corrections for separated flows were developed first by Maskell [3]. His analysis was originally derived for circular plates normal to the flow and is based on conservation of momentum. Recently, a semi-empirical correction was proposed by Mercker [4], which for the first time introduced additional blockage effects associated with the pressure gradient along the test section at empty condition. The purpose of the present study is to investigate the closed wall wind tunnel blockage effect on full-scale heavy-duty truck by using CFD, to assess the blockage correction equations for real vehicle model, and to determine blockage free aerodynamic drag.

2. NUMERICAL METHODS

2.1 Governing Equations and Discretization:

The governing equations being solved in the LES are spatially filtered continuity and Navier-Stokes equations:

$$\frac{\partial \bar{u}_i}{\partial x_i} = 0\,, \tag{1}$$

$$\frac{\partial \bar{u}_i}{\partial t} + \frac{\partial}{\partial x_j}\bar{u}_i\bar{u}_j = -\frac{\partial \bar{P}}{\partial x_i} + 2\frac{\partial}{\partial x_j}\left(\nu + \nu_{SGS}\right)\bar{S}_{ij}\,, \tag{2}$$

The bar over the physical quantity indicates the spatial filtering operation for LES. The filtered strain rate tensor $\bar{S}_{ij}$ and pressure $\bar{P}$ in Eq. (2) are expressed as

$$\bar{S}_{ij} = \frac{1}{2}\left(\frac{\partial \bar{u}_j}{\partial x_i} + \frac{\partial \bar{u}_i}{\partial x_j}\right), \tag{3}$$

$$\bar{P} = \bar{p}/\rho + \left(\overline{u_i u_j} - \bar{u}_i\bar{u}_j\right)/3\,, \tag{4}$$

In Eq. (2), the last term on the right represents the effect of subgrid-scale (SGS) turbulence, which was modeled under the eddy viscosity assumption. The conventional Smagorinsky model (Smagorinsky. 1963) was used, and the eddy viscosity coefficient was modeled as

$$\nu_{SGS} = \left(C_s f_d \Delta\right)^2 \sqrt{2\bar{S}_{ij}\bar{S}_{ij}}\,, \tag{5}$$

where Δ is the length scale of the SGS turbulence expressed as the cube root of each numerical mesh, and model coefficient C_s is set to 0.15, which is generally suitable for external flows. The damping of the turbulent effect near a wall boundary is explained by the Van-Driest type damping function as follows:

$$f_d = 1 - \exp\frac{-l^+}{25}\,, \tag{6}$$

where l^+ is the distance from the wall in wall coordinates.

The governing equations were discretized by using the vertex-centered unstructured finite volume method. The second-order central differencing scheme was applied for the spatial derivatives and blending of 5% first-order upwind scheme for the convection term was employed for numerical stability. The third-order upwind scheme was adopted for the spatial derivative far away from vehicle, where coarser grid was allocated. For time marching, the third-order Adams-Moulton semi-implicit scheme was used. Pressure-velocity coupling was preserved by using the Simplified Marker and Cell (SMAC) algorithm. The pressure Poission equation was solved by the incomplete Cholesky conjugate gradient (ICCG) method.

2.2 Target Vehicle Model:

The configuration of the two different full-scale heavy-duty trucks is shown in Figure 1.The surface of the vehicle is reproduced by about 1.5 million triangle meshes. To reproduce the fine structure, the surface resolution is around 5 to 10 mm around the side mirror, and relatively fine elements are allocated around the cabin. The engine and power train is reproduced by the moderate elements with the resolution of 20 to 50 mm. Larger elements are allocated to reproduce the cargo panel. The triangle element on the surface of the vehicle is indicated in Figure 2. The fluid space was decomposed by tetrahedral elements. To maintain finer resolution around the vehicle, hierarchical allocation is carried out, as shown in Figure 3. Figure 4 illustrates two models with and without air deflector. These two models are used to validate the numerical method.

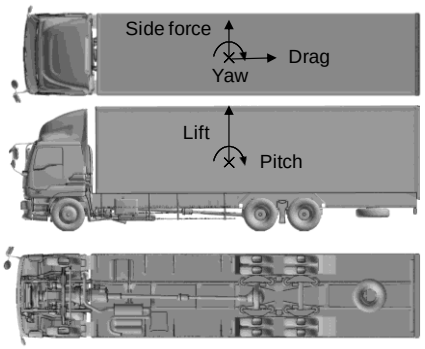

Fig 1. Full-scale heavy-duty truck

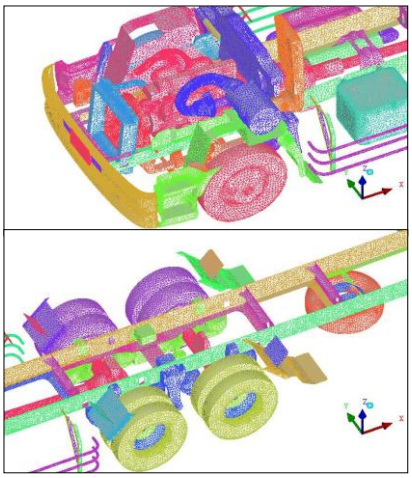

Fig 2. Surface elements on the vehicle

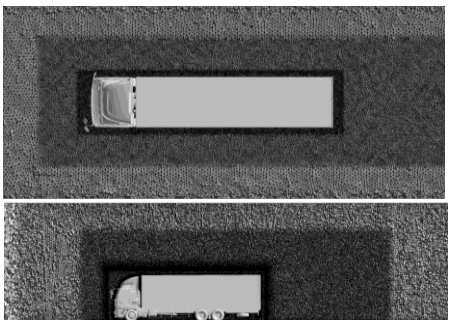

Fig 3. Spatial elements around the vehicle

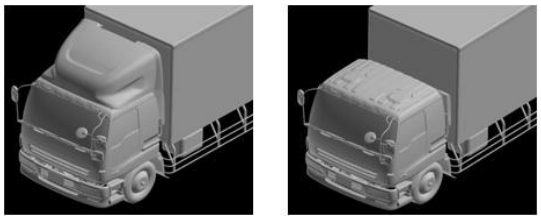

Fig 4. Models with and without the air deflector

2.3 Computational Domain and Boundary Condition:

To validate our numerical method based on the experimental wind tunnel data, we adopted the same wind tunnel geometry in the simulation, as shown in Figure 5(a), in which the blockage ratio of the projected frontal area of the vehicle and the cross sectional area of the test section is about 10%. In the real road condition, blockage effect does not exist. To simulate such a condition, we created a numerical domain with negligible blockage ratio. Hence, we termed this condition an ideal condition, which has the blockage ratio of around 1%, as shown in Figure 5(b).

(a)

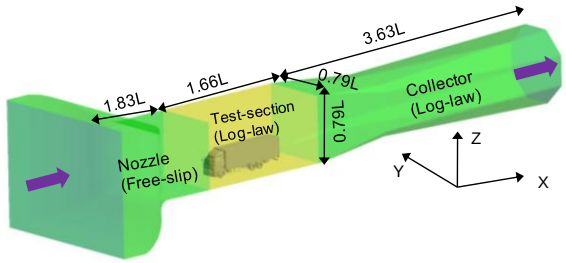

(b)

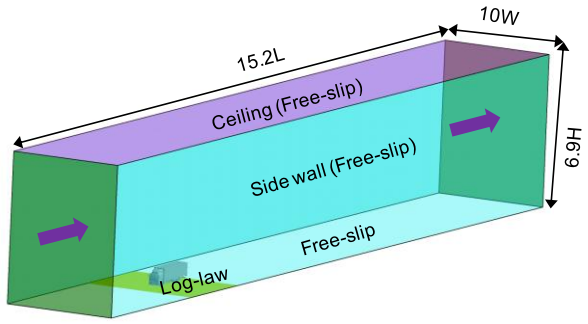

Fig 5. Computational domains: (a) Real wind tunnel geometry, (b) Ideal

In both cases, a uniform velocity distribution U_0 is defined at the inlet (about 22 m/s and 25 m/s in the real wind tunnel and ideal cases, respectively) about 40 m upstream of the vehicle. All velocity components were gradient-free for the steamwise direction at the outlet. Solid wall condition was adopted on the surface of the vehicle body and the floor on which the vehicle was mounted. It was impossible to resolve the entire boundary layer at a reasonable computational cost, especially in the vicinity of the solid wall where large velocity gradient appears. The log-law profile was assumed on the velocity and surface friction on the wall was estimated and directly imposed as Neumann boundary condition. As a result of the assumed log-law profile, the first nearest grid point was allocated so as to maintain the distance from the wall less than about 200 in wall unit (y+), which are located within the logarithmic layer of the boundary layer. In real wind tunnel case, as shown in Figure 5(a), the exit of the wind tunnel nozzle is located 3.79 m windward of the vehicle and the collector is mounted after the test section.

3. Review of Wind-Tunnel Blockage Correction Equations

It is defined that the total blockage correction factor is the sum of velocity acceleration (blockage factor) caused by solid and wake blockage; however these are more difficult factors to assess for unusual geometries such as the heavy-duty truck with including complicated detail characteristics features and the associated flow fields around them.

Maskell [3] was the first to address the problems with non-streamline flow bodies, such as bluff-body testing in closed-wall wind tunnel. Maskell's theory is derived on the basis that the test specimen (i.e. circular flat plate) was located at the center of the test section. The correction of the dynamic pressure ratio is as follows:

$$\frac{q_c}{q} = \left[1 + \frac{5}{2} C_{Duw} \left(\frac{A_M}{A_N}\right)\right], \tag{7}$$

$$C_{Dw} = C_{Duw} / \left(q_c / q\right), \tag{8}$$

where q_c is corrected dynamic pressure, q is uncorrected dynamic pressure, A_M is flat plate area, and A_N is wind tunnel working section cross sectional area.

Mercker [3] provides a blockage correction equation based on the work of Lock [6] for solid blockage and on the work of Maskell [3], Thom [7], and Glauert [8] for wake blockage. Mercker's correction considers the effects of yaw angle, vehicle geometry, and wind tunnel geometry. The correction expressed by the ratio of dynamic pressure as follow:

$$\frac{q_c}{q} = \left[1 + K_3 \tau' \frac{2A_{M\psi}.2V_M}{\sqrt{L_p.2V_M.(2A_N)^{3/2}}} + \frac{2A_M}{2A_N}.\left(\frac{1}{4} C_{Dm}(0) + \eta \frac{2A_{M\psi}}{2A_N}\right)\right]^2 \tag{9}$$

where ε_s is solid blockage factor, ε_w is wake blockage factor, $A_{M\psi}$ is vehicle frontal area at ψ deg. yaw angle, V_M is vehicle volume, and $C_{Dm}(0)$ is the measured drag coefficient at 0 degree yaw angle. Mercker recently modified his procedure in order to consider the static pressure change over the test section at empty state. In closed-wall wind tunnel the aerodynamic drag is strongly influenced by two factors, which are related to tunnel pressure gradient. First one is horizontal buoyancy corrections due to empty tunnel gradients over the model. This buoyancy effect is not important unless the model is

very long. Secondly, wind distortion correction arising from the gradient correction over wake (wake distortion correction) to the measured drag. The wake distortion correction is rarely a problem in closed tunnels, unless the model is long or tested far back in the test section. There is no general theoretical approach has been found to correct for the effects of a pressure gradient on the wake of the bluff shapes that are typical of automobiles. A new semi-empirical approach (Equation 12.) is presented by Mercker [4] that is based on the observation that the drag changes due to a pressure gradient over a wake correlate difference between the base of the vehicle and the position of wake closure.

The drag coefficient is fully corrected in order to consider wake distortion and horizontal pressure buoyancy by

$$C_{DT} = C_{Duw} + \Delta C_{pw} + \Delta C_{DHB} \ , \tag{10}$$

$$C_{Dw} = C_{DT} / (q_c / q) \ , \tag{11}$$

Wake distortion term:

$$\Delta C_{pw} = (C_{pwc} - C_{pmb}) \ , \tag{12}$$

where C_{pwc} is the pressure coefficient in empty wind tunnel at the location of wake closure and C_{pmb} is the pressure coefficient in empty wind tunnel at the location of the base of the model.

Drag correction due to the horizontal buoyancy is expressed as:

$$\Delta C_{DHB} = [1.75 / A_M][V_M / 2]G \ , \tag{13}$$

$$G = \left[(dcp/dx)_n + (dcp/dx)_c \right], \tag{14}$$

where G is the Glauert factor, $(dcp/dx)_n$ denotes the static pressure gradient at nozzle side and $(dcp/dx)_c$ denotes the static pressure gradient at collector side.

4. RESULTS AND DISCUSSION

4.1 Validation of the Numerical Method

The numerical method was validated in the present study by comparing the LES results obtained in stationary cases to wind tunnel measurements. The wind tunnel experiment was conducted at DNW, which has a test section of 20 m × 9.5 m × 9.5 m for the length, width, and height respectively. The same Reynolds number (inlet velocity) and full scale heavy-duty truck model as in the LES were used. Two models with and without the air deflector are compared here. For comparison purposes, we calculate the time-averaged drag coefficient, defined as $C_d = F_d / (\frac{1}{2} \rho A_M U_{inlet}{}^2)$ and lateral force coefficient, defined as $C_s = F_s / (\frac{1}{2} \rho A U_{inlet}{}^2)$. The errors of the LES results with respect to the experimental data are summarized in Table 1. It should be reminded here that we used exactly same grid resolution around the vehicle for all cases, thus the numerical error included in the results is exactly the same. For the model with the air deflector, the LES underestimates the drag in the real wind tunnel geometry condition by 8%. In the same way, the LES underestimates the drag in the model without the air deflector in the real wind tunnel geometry by 11%. On the other than, LES result achieved good agreement in lateral force for both models. Finally, it should be noted that the effect of drag reduction by the air deflector identified in the wind-tunnel experiment is 16.5%, while that in the LES is 15%, indicating that accuracy of our LES is satisfactory.

Table 1: Drag coefficient (C_d) and lateral force coefficient (C_s) deviation from experiment

Deviation from Expt. (%)	C_d	C_s
Model with the air deflector	-8 %	negligible
Model without the air deflector	-11 %	negligible

4.2 Empty Tunnel Simulations

The DNW geometry wind tunnel consisted of a 9.5 m × 9.5 m test section which has a length of 20 meters as shown in Figure 5(a). The upstream region of the nozzle gradually decreases from a circular cross-section to a rectangular cross-section up to beginning of test section. The test section has uniform rectangular cross-section. The downstream region of the test section has a convergent-divergent type collector. From empty wind tunnel simulation we observed that pressure gradients were occurred over the test section due to boundary layer development and steep gradient on the wake region due to collector geometry. In closed-wall wind tunnel blockage correction usually consists two parts: a correction to the measured dynamic pressure (q-correction) and a gradient correction. The purpose of empty tunnel simulations to discern the blockage mechanism due to non-uniform streamwise pressure gradient correction.

4.3 Evaluation of the Correction Equation

The time-averaged aerodynamic drag coefficient shown in Table 2 was obtained by real wind tunnel geometry and ideal condition wind tunnel simulation for the model with air deflector. In this paper, all the drag coefficient of the models, with and without air deflector, are normalized by the corresponding models' drag coefficient obtained numerically with the real wind tunnel geometry, at 0 degree yaw. In Table 3, the aerodynamic drag is corrected by Maskell and Mercker methods.

The corrected results were obtained by using drag coefficient from real wind tunnel geometry simulation. In the present study, we use the drag coefficient obtained under the ideal condition as the baseline to verify the correction equations. Hence the object is to identify

which correction equations show a better agreement with the ideal drag coefficient.

The corrected value by Mercker's method shows good agreement when considering only the solid blockage, wake blockage and horizontal buoyancy terms. Also Maskell's correction equation has a similar trend in 0 degree yaw and it shows over correction in 10 degree yaw. On the other hand, when taken into account all of the effects including wake distortion term in the Mercker's method, drag is overcorrected.

Table 2: Normalized drag coefficient for the model with air deflector (0 and 10 degree yaw angle)

Normalized drag coefficient (CFD)		
Yaw angle(deg.)	DNW geometry	Ideal LES
0	1.000	**0.801**
10	1.716	**1.297**

Table 3: Normalized corrected drag coefficient for the model with air deflector by correction Equation (0 and 10 degree yaw angle)

Normalized Corrected Drag coefficient based on Mercker Eq.		
Factors considered	0 deg.	10 deg.
Solid + Wake blockage	0.847	1.329
Solid + Wake blockage + HPB	**0.789**	**1.278**
Solid + Wake blockage + HPB + Wake distortion	0.693	1.189

Normalized corrected Drag coefficient based on Maskell Eq.		
Factor considered	0 deg.	10 deg.
Solid blockage	0.787	1.174

Table 4 and Table 5 present the result obtained with model without the air deflector at 0 degree yaw. We can see that aerodynamic drag corrected by Mercker's method shows a better agreement when excluding the wake distortion effect. The corrected result by Maskell's method shows the over correction to compare with ideal result. From our CFD results, we realize that Maskell's method shows the worst result in non-zero yawing.

Concerning the relatively large discrepancies between the ideal drag coefficient and the corrected drag coefficient by Maskell's method, one possible explanation is that the Maskell's correction equation is based on simplified geometry (symmetric wake structure at rear section of a circular flat plate) and do not account for the effect of yawing. To consider the wake distortion in Mercker's method, which depends on approximation location of the wake closure, the relevant length behind the vehicle over which the pressure gradient effect has to be calculated. This location is measured up to a first order of approximation, which occurs where $\Delta C_{PT} = 0$, here C_{PT} is total static pressure coefficient. Recently, Mercker [4] has noticed that the true length (sensitivity length) can be determined exactly by generating a second gradient in the empty test section. It is turned out that this length is usually shorter than the distance between vehicle base location and wake closure location. For that reason, when using the wake closure location, the buoyancy effect on the wake overcorrected the measured drag coefficient. We can say that at this moment we are yet in the position to determine the sensitivity length on a pure theoretical base other than on experimental grounds.

Table 4: Normalized drag coefficient for the model without air deflector (0 degree yaw angle)

Normalized drag coefficient (CFD)		
Yaw angle(deg.)	DNW geometry	Ideal LES
0	1	**0.812**

Table 5: Normalized corrected drag coefficient for the model without air deflector by correction Equation (0 degree yaw angle)

Mercker		Maskell
Factors considered	0 deg.	0 deg.
Solid + Wake blockage	0.848	0.764
Solid + Wake blockage + HPB	**0.802**	
Solid + Wake blockage + HPB + Wake distortion	0.762	

5. WAKE STRUCTURE

To investigate the tunnel pressure gradients, we visualize the flow structures over the near wake region by total pressure coefficient. Snapshots of wake structures around the rear-end of the vehicle at 0 degree and 10 degree yaw angle are shown in Figure 7 and Figure 8 respectively. Figure 7 shows the wake structure (upper figure) at DNW geometry for the model with air deflector at 0 degree. In DNW geometry simulation, we can see that the wake is more or less distorted by the presence of pressure gradients and wake is extended in longitudinal direction as well as in vertical direction. In ideal case simulation, the wake structure is not affected by the pressure gradients and wake is formed freely. However, when a non-uniform, streamwise pressure distribution was introduced, an increase of the up to 101 drag counts and 92 drag counts were measured at 0 degree and 10 degree yawing respectively. While the pressure gradient extended over both the solid part of the vehicle model and the wake, the solid-body buoyancy only explained approximately one-half of the drag change. Therefore, it was concluded that the remaining drag coefficient difference was investigated by the wake being distorted by the tunnel pressure gradient.

Mercker proposed wake distortion correction is empirical and wake distortion is related to the change in base pressure. The actual mechanism by which this occurs is unknown [3], but the phenomena has been realized for a wide range of vehicle geometries from very simplified automotive shapes to full-scale vehicle models, to normal flat plate in different wind tunnels. At present, the only piece of information required to apply the correction is the magnitude of a wake parameter that relates to the length of the wake separation bubble at

rear-end of the model.

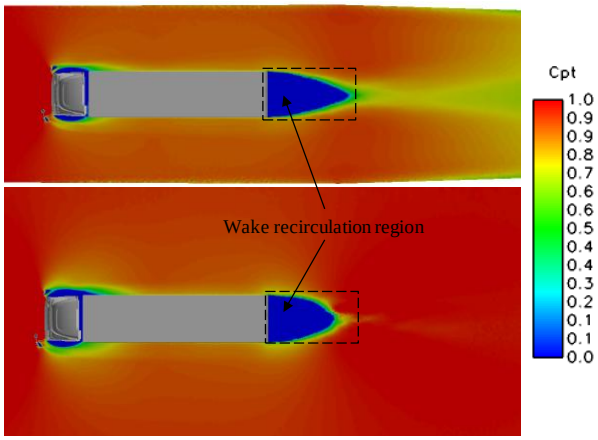

Fig 7. Wake total pressure distribution at 0 degree yawing (Above: DNW geometry, Below: Ideal)

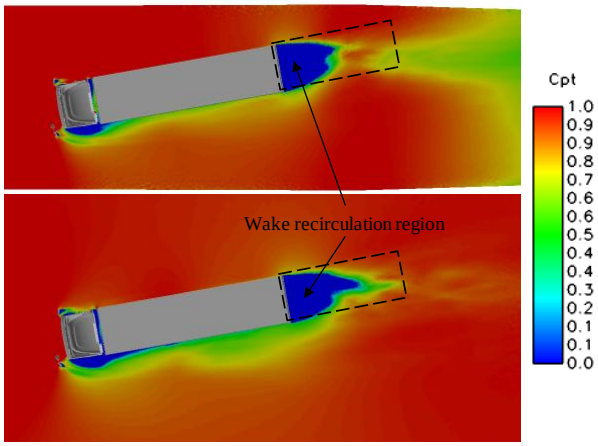

Fig 8. Wake total pressure distribution at 10 degree yawing (Above: Real wind tunnel geometry, Below: Ideal)

6. CONCLUSIONS

Large-eddy simulations have been performed successfully to assess the wind tunnel blockage effects on full-scaled, heavy-duty truck models. The Maskell's correction equation for aerodynamic drag is working well for the model with the air deflector without considering the yawing effect. The drag coefficients under the effect of yaw angle obtained with the correction method proposed recently by Mercker had shown good agreement with the ideally obtained values in both models. But further investigation is needed for wake induced drag increment for steep pressure gradient in Mercker's procedure.

This study has dealt with two specific full-scale vehicle models in closed-wall wind tunnel geometry at different yaw angles. It is expected that the correction procedure is applicable to any vehicle shape and various wind tunnel geometry when the rear-end wake bubble is influenced by tunnel pressure gradient.

ACKNOWLEDGEMENT

This work was supported by the Industrial Technology Research Grant Program in 2007 from the New Energy and Industrial Technology Development Organization (NEDO) of Japan. This study was conducted in a collaborative research project with Isuzu Advanced Engineering Center Ltd., and the geometry data and experimental data received are greatly acknowledged.

7. REFERENCES

1. Hucho, W.H. "Aerodynamic of Road Vehicles" Fourth Edition, 1998.
2. K.R. Cooper et al. "Closed-Test-Section Wind Tunnel Blockage Corrections for Road Vehicles", SAE International. SP-1176.
3. Maskell, E.C. "A Theory of the Blockage Effects on Bluff Bodies and Stalled Wings in a Closed Wind Tunnel", ARC R&M 3400, Nov. 1963.
4. E. Mercker et al. "The Influence of a Horizontal Pressure Distribution on Aerodynamic Drag in Open and Closed Wind Tunnels", SAE 2005-01-0867, 2005.
5. E. Mercker. BMW AG, Germany and Dr. Koro Kitoh, Kozo Kitoh Technology. Inc, 2011: Private communication.
6. Lock, C.N.H. "The Interference of a Wind Tunnel on a Symmetrical Body", ARC R&M 1275, 1929.
7. Thom, A. "Blockage Corrections in a Closed High Speed Tunnel", ARC R&M 2033, Nov. 1943.
8. Glauert, H. "Wind Tunnel Interference on Wings, Bodies and Airscrews", ARC R&M 1566, 1933.
9. Smagorinsky, J. "General circulation experiments with the primitive equations, 1. The Basic Experiment. Monthy Weather Review" 91 (3), 99-164, 1963.

8. NOMENCLATURE

Symbol	Meaning	Unit
C_d	Drag coefficient	[-]
F_d	Drag force	[N]
C_s	Lateral force coefficient	[-]
F_s	Lateral force	[N]
ρ	Air density	[kg/m^3]
A_M	Vehicle frontal area	[m^2]
U_{inlet}	Inlet velocity	[m/s]
C_{DT}	Total drag coefficient	[-]
C_{Duw}	Measured drag coefficient	[-]
C_{Dw}	Corrected drag coefficient	[-]
G	Glauert factor	[-]

9.MAILING ADDRESS

Prasanjit Das
Graduate School of Engineering
Computational Fluid Mechanics Laboratory
Hokkaido University
Kita 13, Nishi 8, Kita-Ku, Sapporo, Japan
E-mail: prasanjitd11@yahoo.com